
FoveaTer: Foveated Transformer for Image Classification

Aditya Jonnalagadda¹, William Wang³, Miguel P. Eckstein^{1,2}

¹Electrical and Computer Engineering, ²Psychological and Brain Sciences, ³Computer Science,
University of California, Santa Barbara, CA, USA
aditya_jonnalagadda@ece.ucsb.edu, william@cs.ucsb.edu, eckstein@psych.ucsb.edu

Abstract

Many animals and humans process the visual field with a varying spatial resolution (foveated vision) and use peripheral processing to make eye movements and point the fovea to acquire high-resolution information about objects of interest. This architecture results in computationally efficient rapid scene exploration. Recent progress in vision Transformers has brought about new alternatives to the traditionally convolution-reliant computer vision systems. However, these models do not explicitly model the foveated properties of the visual system nor the interaction between eye movements and the classification task. We propose foveated Transformer (FoveaTer) model, which uses pooling regions and saccadic movements to perform object classification tasks using a vision Transformer architecture. Our proposed model pools the image features using squared pooling regions, an approximation to the biologically-inspired foveated architecture, and uses the pooled features as an input to a Transformer Network. It decides on the following fixation location based on the attention assigned by the Transformer to various locations from previous and present fixations. The model uses a confidence threshold to stop scene exploration, allowing to dynamically allocate more fixation/computational resources to more challenging images. We construct an ensemble model using our proposed model and unfoveated model, achieving an accuracy 1.36% below the unfoveated model with 22% computational savings. Finally, we demonstrate our model's robustness against adversarial attacks, where it outperforms the unfoveated model.

1 Introduction

Many mammals, including humans, have evolved a locus (the fovea) in the visual sensory array with increased spatial fidelity and use head and eye movements [1, 2] to orient such locus to regions and objects of interest. The system design allows visual-sensing organisms to accomplish two objectives: fast target detection crucial for survival and savings in the computational cost. Computational savings are accomplished by limiting the number of units with high computational costs (i.e., higher spatial resolution processing) to a small spatial region, the fovea. Fast target detection is achieved by distributing the remaining computational power across a much larger area in the periphery, with a lower spatial resolution with increasing distance from the center of the fovea. Critical to the design is an efficient algorithm to guide through eye movements the high-resolution fovea to regions of interest using the low-resolution periphery [3, 4, 5] and allow optimizing the target detection and scene classification. Various computational models were proposed to model the search using foveated visual system [6, 7].

Computer vision has evolved from using hand-crafted features to data-driven features in modern CNNs. Due to their computational limitations, the objectives of the computer vision systems align well with the human visual system. Approaches towards saving computational power can be seen, for example, computer vision systems evolved from using sliding windows to RCNN's [8] use of selective

search and Faster-RCNN’s [9] use of Region Proposal Network (RPN). Approaches to exploring the scene can be seen in models like RAM [10] where they sequentially process the image and decide what to process next by using the peripheral information. Saliency-based models [11, 12, 13] try to find the target using low-level features.

The recent innovation in computer vision of using Transformers [14, 15] for object classification tasks departs from the traditional over-reliance on convolutions. Even after replacing the convolutions with attention modules and multilayer perceptrons, visual Transformers [15, 14] achieve close to state-of-the-art performance on the ImageNet dataset. Transformers [16] have the added benefit of self-attention using which locations far apart in the image will interact with each other. We introduce the concept of foveated vision into transformers, thereby bringing additional potential gains to using transformers. To this end, we perform an object classification task using multiple fixations, moving foveal attention across different parts of the image, and using only a limited portion of the image information at each fixation, thereby reducing the input to the transformer by many folds. The model decides on subsequent fixation locations by using all the visual information gained until the current step. Finally, we integrate information across fixations to make the final classification decision.

2 Related work

Transformers have achieved great success in the field of Natural Language Processing since their introduction by Vaswani et al., [16] for machine translation. Recently, the application of Transformer models in computer vision has seen tremendous success. Vision Transformer (ViT) model introduced by Dosovitskiy et al., [15] achieved remarkable performance on ImageNet [17] by using additional data from JFT 300M [18] private dataset. Subsequently, the DeiT model [14] introduced the concepts of knowledge transfer in transformers for leveraging the learning from existing models. Using augmentation and knowledge transfer, the DeiT model achieved close to state-of-the-art performance using training data from the ImageNet dataset alone.

Sequential processing provides three main advantages in computer vision. Larochelle and Hinton 2010 [19] proposed a model based on the Boltzmann machine that uses foveal glimpses and can make eye movements. First, it can limit the amount of information to be processed at a given time instant to be constant, i.e., the ability to keep computations constant irrespective of the input image size. Second, sequential models can help model human eye movement strategies and help transfer that information to build better computer vision systems. RAM [10] introduced a sequential model capable of making a sequence of movement across the image to integrate information before classification. In addition, the hard-attention mechanism, implemented using reinforcement learning, was used to predict consequent fixation locations. Ba and Minh [20] extended these ideas to recognize multiple objects in the images on a dataset constructed using MNIST. Third, sequential processing requires fewer parameters than a model using full-resolution image input. Other models [21] proposed image captioning models based on both hard-attention and soft-attention. Visual attention was also used for other applications [22, 23].

Various computational models have been proposed for rapid categorization in terms of low-level properties such as spatial envelopes [24] texture summary statistics [25]. Saliency-based models [11, 12, 13] traditionally tried to model eye movements by identifying bottom-up properties in the image that will capture attention. Torralba et.al [26] showed how saliency could be combined with contextual information to guide eye movements. Freeman and Simoncelli proposed a biologically-inspired foveated architecture [27], an average-pooling based model used to approximate various stages of visual processing and the size of the receptive field used for average-pooling increased with distance from the point of fixation. That model was integrated with a deformable parts model to build a foveated object detector [28].

FoveaTer combines an approximation to biologically-inspired foveated architecture with a Vision Transformer Network. We apply our model to real-world images from the ImageNet dataset for the task of image classification. Input to the transformer is foveated using the pooling architecture described in the following sections basing on the fixation location, which results in a reduction in the number of inputs to the transformer. The subsequent fixation location is given by a confidence map, constructed using the attention weights from the last transformer block. Feature vectors corresponding to class tokens from different fixations are combined using another transformer block, resulting in the final classification decision. Our model also understands that all images are not equally difficult to

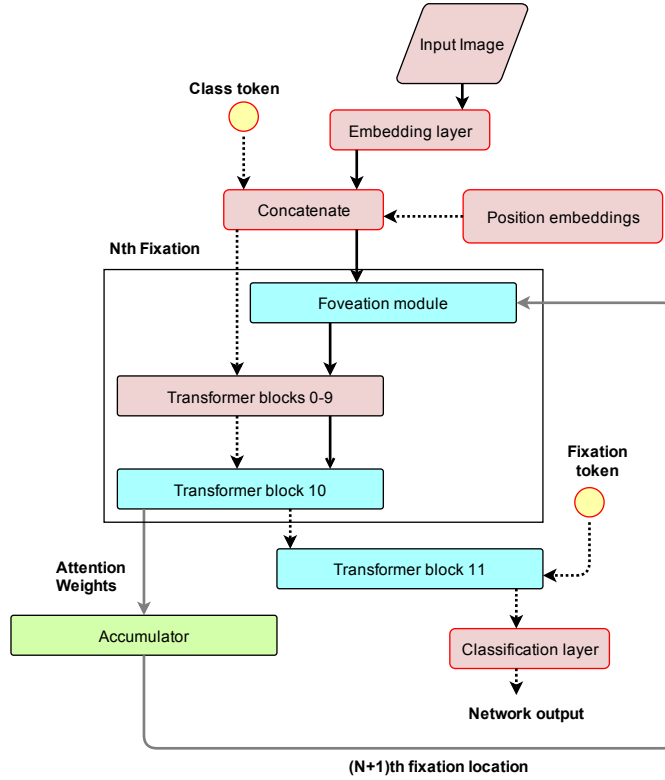


Figure 1: **FoveaTer architecture:** Solid black arrows denote the flow of image-related features. The Foveation module pre-processes the full-resolution features resulting in increased pooling of features with distance from the fovea. Pooled features are the input to the transformer. Two types of tokens are used. Default class token is accompanied by a newly introduced fixation token, which is given as input to block 11 along with block 10 output corresponding to class token from all fixations. Output of block 11 corresponding to fixation token is used for classification.

classify and that varying computational resources can be used to classify different images successfully. The model implements this idea using a confidence threshold to restrict the scene exploration to the necessary fixations to classify the image. Finally, we overcome the expected drop in performance due to limiting our model to localized attention interactions using an ensemble model of FoveaTer and a full-resolution Vision Transformer for images where the FoveaTer gives low confidence output. Our source code location and description are available in Appendix.

3 Model overview

Our model inherits the Vision Transformer architecture, and it is shown in Figure 3. The input image to the model is separated into patches and then encoded into embedded features using embedding layer and added to positional embeddings. We introduce a foveation module that transforms the full-resolution feature embeddings into pooled features using average pooling. Attention weights from the penultimate transformer block are used as input to an accumulator to generate a confidence map capable of predicting the next fixation location. We introduce a new fixation token for the final transformer block, which interacts with the penultimate transformer block outputs corresponding to the class token from all the fixations. Final blocks output corresponding to the fixation token is used as input to the final classification layer.

Embedding layer The input image of size [3, 224, 224] is separated into image patches of size [3, 16, 16] pixels and passed through an embedding layer to generate the embedded feature vectors. Since

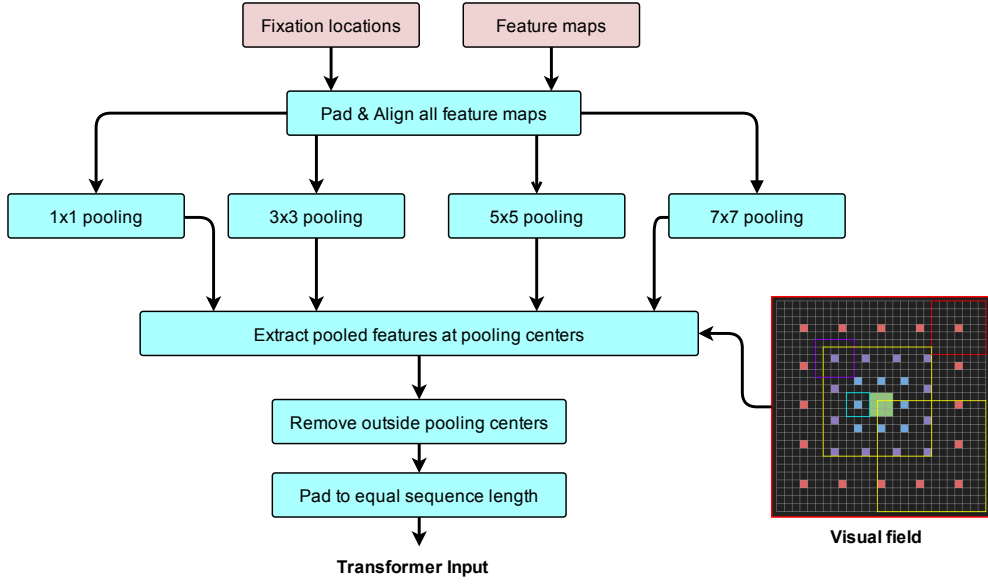


Figure 2: **Foveation module:** Input features with different fixation locations are padded and aligned to the visual field. Then, average pooling with varying kernel sizes is performed, and pooled features corresponding to pooling region centers are extracted. Finally, pooled features falling outside the image are ignored, and pooled features are padded to a constant sequence length of 29 and is given as input to the transformer.

the dataset and image size are the same for the pre-trained model, we use the pre-trained parameters from the model for the embedding layer and position embedded features.

Foveation module Inspired from the radial-polar pooling regions proposed in [27], we use squared pooling regions in this paper for computational speed-up. Each image in a mini-batch has its fixation location, and since the pooling is fixation-dependent, each image needs to be pre-processed individually. Whereas, for the case of square pooling regions, we can make use of PyTorch library functions. However, due to the unavailability of library functions for radial-polar pooling regions, processing speed becomes much slower. We optimized our code to minimize the latency introduced by the Foveation module.

Figure 2 shows the visual field of the foveation module. Highlighted regions correspond to the centers of the pooling regions, 49 blocks. We use pooling regions with receptive field sizes 1x1, 3x3, 5x5, 7x7 blocks, where block corresponds to a receptive field of [16,16] pixels in the input image of width and height 224. Central green 3x3 block represents the high-resolution fovea where no average-pooling is done, and high-resolution features are retained. The next ring of pooling regions where the center of the pooling region is represented with blue has a receptive field of 3x3 which translates to average-pooling of 9 feature vectors to generate the representative feature vector for that pooling region. Similarly, the rings of violet and red-colored pooling centers have receptive fields of 5x5 and 7x7 blocks, respectively. Yellow squares are of size 14x14 blocks, giving an idea of image size to the visual field. In terms of the fraction of area occupied, the image occupies 26.89% of the visual field, whereas the pooling regions with receptive field sizes 1, 3, 5, 7 occupy 0.14%, 1.24%, 3.43%, 6.72% respectively. The output of a pooling region is constructed by average-pooling all the feature vectors falling inside the pooling region. We ignore the pooling regions falling outside the image, and the output of the foveation module is zero-padded to maintain the same length across all images present in a batch since different fixation locations give rise to an unequal number of active pooling regions. We use 29 as the feature length as it is the maximum possible number of active

pooling regions.

$$P_i = (1/M) \sum_{j=0}^{M-1} E_{ij} \quad (1)$$

Where $i = \{1, \dots, 49\}$ corresponds to the pooling region index, E_{ij} is the embedded feature vector present in that pooling region, $M = \{1, 9, 25, 49\}$ corresponds to number of features inside the pooling region and P_i is the mean feature vector corresponding to that pooling region.

Transformer We use DeiT-Tiny architecture [14] for constructing the transformer. We add two additional transformer blocks and make two blocks of the default architecture as identity layers, resulting in the same number of parameters as the default model. We use the penultimate block to get the attention weights corresponding to how the feature vectors are weighted to get the feature vector corresponding to the class token. A new token called fixation token is introduced at the last transformer block. The output corresponding to the class token from the penultimate block from all fixations is given as input to the final block along with the fixation token. The output corresponding to the fixation token is used as input to the classification layer.

Predicting next fixation location Attention weights from the penultimate block are collected to get each pooling region’s contribution to the feature vector corresponding to the class token. A confidence map is constructed by putting these weights back on a 14x14 map at the corresponding pooling region’s location based on the point of fixation. Inhibition of return (IOR) [29] refers to a tendency in human observers not to attend at previously attended or fixated regions. Here we constructed a map by applying an IOR of 3x3 blocks around a fixation location. After each fixation, the IOR map is degraded by 50%. After subtracting the IOR map from the confidence map, the max location in the resultant map is used as the next fixation location.

Loss function We use Cross-entropy for computing the classification loss. Loss from all fixations ($i=1,5$) is incorporated to get the mini-batch loss, as shown below.

$$loss = \sum_{i=1}^5 \sum_j y_j \log(P(y_j)) + (1 - y_j) \log(1 - p(y_j)) \quad (2)$$

Where $i = \{1, 2, 3, 4, 5\}$ corresponds to the fixation index, y corresponds to the target label, j corresponds to the class index and P corresponds to the predicted probability.

Algorithm 1: Model Overview

Result: Classification decision

$E = \text{Embedded_layer}(\text{Input_Image});$

$EP = E + \text{position_embeddings};$

Initialize random fixation location $F_{xy};$

$T_out = \text{fixation_token};$

while $\text{current fixation} < \text{total fixations}$ **do**

 Foveate features: $F = \text{Foveation_module}(EP, F_{xy});$

for $idx \in \text{range}(10)$ **do**

$F = \text{Transformer_block}_{idx}(F)$

end

 Extract attention: $F, \text{attn_wts} = \text{Transformer_block}_{10}(F);$

 Update accumulator(A) with $\text{attn_wts};$

$T_out = \text{Concatenate}(T_out, F_0);$

$Y = \text{Transformer_block}_{11}(T_out);$

$\text{logits} = \text{classification_layer}(Y);$

 Next Fixation: $F_{xy} = \text{MAX}(A \text{ with } \text{IOR});$

end

4 Experiments

4.1 Implementation details

Training: We follow the training schedule suggesting in the DeiT paper. AdamW [30, 31] optimizer with a decay of $1e - 8$ is used with a cosine learning rate schedule. We train all the 5.5M parameters of the model except for the embedding layer and position embedding, as stated above. Initial learning was set at $1e - 5$, and the minimum learning rate was set at $1e - 6$. Both foveated and unfoveated models were trained for 75 epochs. We choose our hyperparameters based on the hyperparameters used during training and fine-tuning phases for DeiT implementation [14] and use the same augmentation techniques. We initialize our model weights with DeiT-Tiny architecture weights. 100 random classes from ImageNet are used for training and testing the model. We use the train validation split provided by the ImageNet split. Regarding the hardware, we use GeForce GTX 1080 Ti for training and testing purposes. Both foveated and unfoveated models take approximately one day to train for 75 epochs. During training, the unfoveated model made five fixations on each input image, with the initial fixation starting at a random location. Due to its flexibility, the same model can be used to make any number of fixations.

Dataset: We consider a subset of the ImageNet dataset for presenting our results. We used 100 random classes from the ImageNet dataset by selecting the first 100 folders in the directory list with coded class names as the folder names, listed in Appendix. Accuracies reported in the following subsections are the performance on the validation set of ImageNet, which was not used during the training phase. Results are reported on the validation set of size 5000 images. Chance value is 0.01.

Cost: Foveated and unfoveated models are designed with the same architecture. However, the foveation module is skipped for the unfoveated model. Computation requirements are determined based on the number of inputs to the transformer blocks. For the unfoveated model, there are 197 inputs, 196 feature vectors, and a class token. Therefore, the unfoveated model incurs a cost of 197 computations. Foveated model has 30 inputs, 29 feature vectors, and a class token. Therefore, each additional fixation incurs a cost of 30 additional computations.

4.2 Predicted fixations Vs Random fixations:

The model starts with an initial random fixation. Under guided fixations, the model uses the attention map computed as described in the previous section. For the random fixation condition, the attention map is replaced with random values. The Foveation module is skipped in the full-resolution model. The unfoveated model has an accuracy of 0.8316. Using the foveated model, the accuracies achieved by making one to five fixations are 0.5432, 0.6874, 0.7236, 0.7366, and 0.7466, respectively, where the first fixation is an initial random fixation and the other four fixations are guided by the model’s accumulator. When we replace the guided fixations with random fixations, the accuracies drop to 0.5334, 0.6168, 0.6468, 0.6654, and 0.6782, respectively. Results are shown in Figure 3.

4.3 Accuracy and Computational savings of the ensemble model:

In this section, we present an ensemble model which tries to maximize the accuracy while minimizing the number of computations required.

We use a combination of our foveated model and the full-resolution model to construct the ensemble model. We use a confidence threshold to determine how many fixations to make on an image and determine if the image needs to be passed through the full-resolution model, which is the final step of the ensemble model due to its high computational cost.

Computing the confidence threshold: We accumulate the probabilities of correct predictions for one guided fixation case, i.e., initial random fixation followed by one guided fixation on the training dataset, compute the mean of those probabilities, and use it as the confidence threshold. Basing on this, we use a threshold of 0.59, which is 59 times higher than the chance probability of 0.01.

We organize our models basing on their computational complexity, i.e., one fixation to five fixations followed by the unfoveated model. As mentioned before, each fixation incurs a computational cost of 30, whereas the unfoveated model incurs a cost of 197. Once the images are processed with a model,

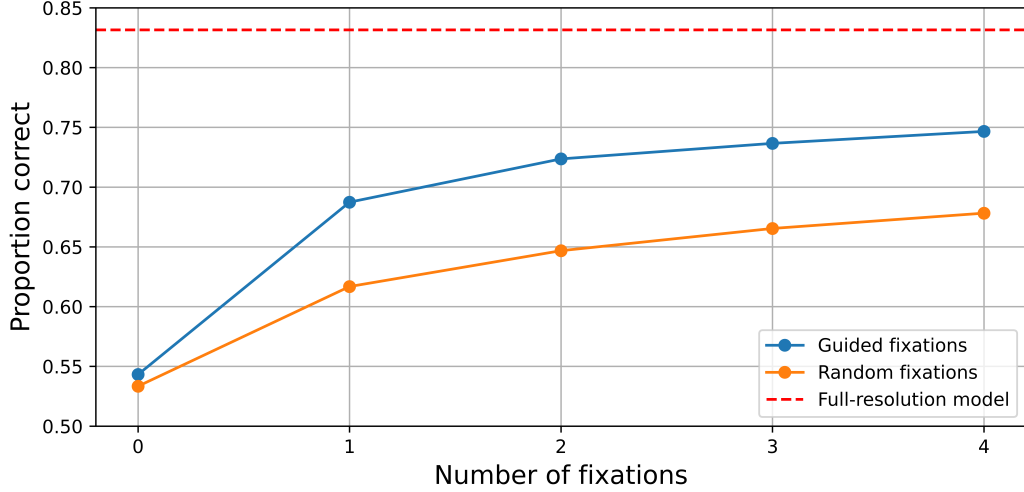


Figure 3: Accuracy comparison of the full-resolution model, foveated model with guided fixations, and foveated model with random fixations.

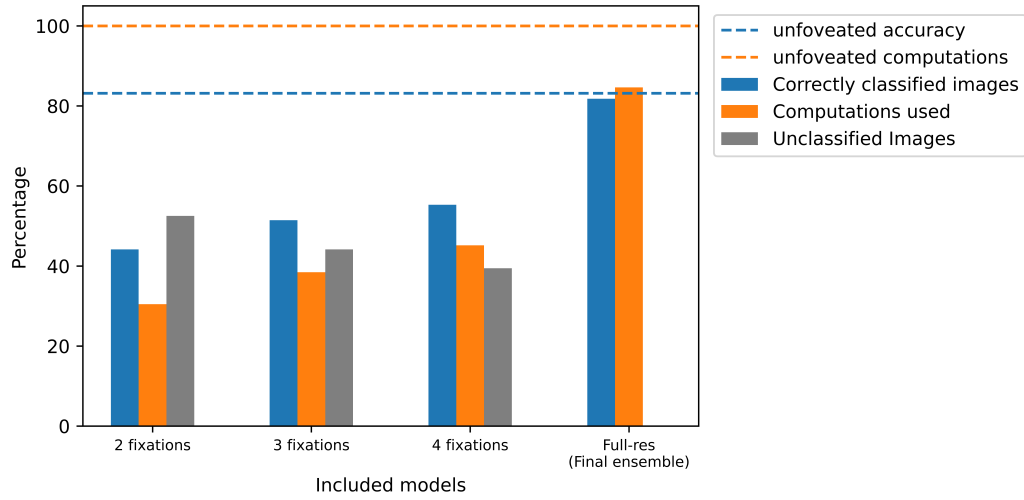


Figure 4: **Ensemble model performance:** Gray bars indicate the percentage of unclassified images, i.e., with a maximum probability below the confidence threshold, blue bars represent the percentage of the correctly classified images, and the orange bar represents the relative percentage of the computations used to the unfoveated model computations.

predictions above the confidence threshold are classified as correct and incorrect classifications. Images with prediction probabilities below the threshold are retained as unclassified images and are processed through the next model. Results with this approach are shown in Figure 4.

Using 78% the computational capacity, the ensemble model achieves an accuracy of 81.8% compared to the unfoveated model’s accuracy of 83.16%, i.e., the ensemble model achieved PC 1.36% below the unfoveated model. A better ensemble model would decrease the gap between unfoveated and ensemble models with the same computational savings.

RAM: Since the foveated model has only 30 inputs, including class token, to the transformer per fixation compared to the 197 inputs for the case of the unfoveated model, foveated model consumes less memory for model training, i.e., 4103 MB for foveated model and 7546 MB for unfoveated model. This allows the possibility of using larger batch sizes.

4.4 Robustness against adversarial attacks

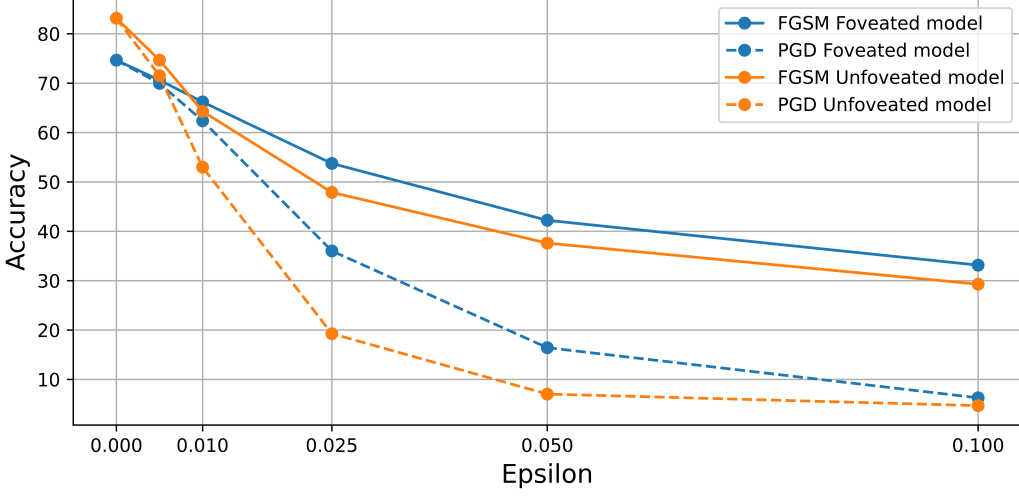


Figure 5: **Adversarial robustness:** Unfoveated and foveated model performance against FGSM and PGD attacks. Epsilon represents the strength of the attack. Although the curves start with unfoveated model performing better than foveated model, as the strength of the attack increases foveated model outperforms unfoveated model.

As shown in some of the previous works [32, 33, 34, 35, 36], we demonstrate the robustness of our foveated system in this section. We consider the two adversarial attacks, Fast Gradient Sign Method (FGSM [37]) and Projected Gradient Descent (PGD [38, 39]), to compare the robustness of foveated and unfoveated models. We use Cleverhans library [40] for implementing the adversarial attacks. The accuracy of the models after the adversarial attack is shown in Figure 5. Epsilon corresponds to the strength of the attack. To compute the adversarial image for both models, position-added embedded features are used as the input to the adversarial network. As it can be observed from the plot, although the performance of the unfoveated model is better than the foveated model to start with, as the strength of the attack increases, the gap decreases, and finally unfoveated model performs better than the foveated model. The robustness of the unfoveated model can be either due to the pooling operations that are part of the model or due to our model’s inherent ability to dynamically decide fixation paths, thereby minimizing the effect of the attack by automatically following a different path from that of the adversarial model. This might help our model provide a better approximation to human performance for certain tasks.

Figure 6 shows some examples of the fixation sequences of the model. Figure 7 shows the visualization of how the image looks to the model at each fixation.

5 Conclusion

We provided a comprehensive framework for using foveal processing on vision Transformers for the task of image classification. Similar to the dependence of the DeiT model on knowledge transfer, our model depends on the ensemble model to reach state-of-the-art performance. As a trade-off, it allows us to limit computations required to process an image by flexibly adjusting the required number of fixations, allowing larger batch sizes during training, providing robustness to adversarial attacks, and giving us a model that can allocate computational resources based on the difficulty of an image.

Future work will work towards replacing the ensemble model with a stand-alone model of FoveaTer. In conclusion, we leveraged the most recent Vision Transformer architecture and combined it with ideas from the foveal vision to come up with a model which has multiple knobs in terms of the number of fixations to be made and limits on the computations done so that the end-user will have the flexibility to fine-tune depending on their needs.

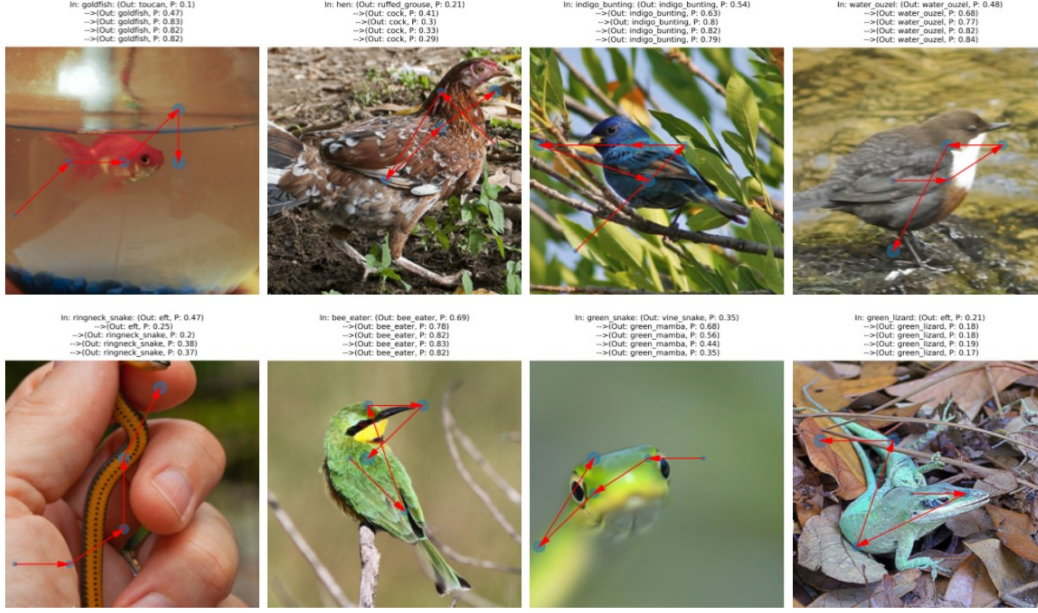


Figure 6: **Fixation sequences:** Five fixations are made for each image, with an initial random fixation followed by four guided fixations. Each subsequent fixation center is represented with a bigger **blue circle**. **Red arrows** represent the transition from one fixation to the next. **In** denotes target class name. **Out** denotes predicted class, and the corresponding predicted probability is shown with prefix **P**. Predicted class label and probability is shown for all the five fixations.

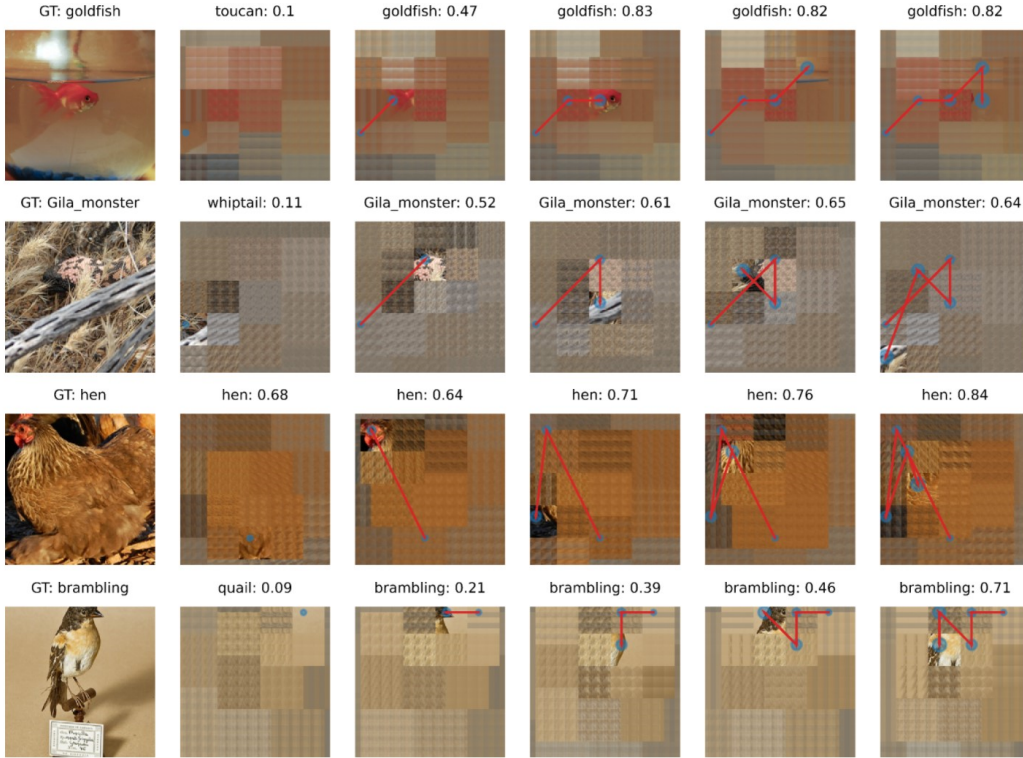


Figure 7: **What the model sees:** Each row contains five images corresponds to the five fixations on a single image. Left-most is the original image with ground-truth (GT) class.

References

- [1] M. Land. Oculomotor behaviour in vertebrates and invertebrates. *The Oxford Handbook of Eye Movements*, 01 2012.
- [2] N Marshall, M. Land, and T Cronin. Shrimps that pay attention: Saccadic eye movements in stomatopod crustaceans. *Philosophical transactions of the Royal Society of London. Series B, Biological sciences*, 369:20130042, 02 2014.
- [3] Mary Hayhoe and Dana Ballard. Eye movements in natural behavior. *Trends in cognitive sciences*, 9(4):188—194, April 2005.
- [4] Hans Strasburger, Ingo Rentschler, and Martin Jüttner. Peripheral vision and pattern recognition: A review. *Journal of vision*, 11:13, 05 2011.
- [5] Casimir J. H. Ludwig, J. Rhys Davies, and Miguel P. Eckstein. Foveal analysis and peripheral selection during active visual sampling. *Proceedings of the National Academy of Sciences*, 111(2):E291–E299, 2014.
- [6] H. Yamamoto, Y. Yeshurun, and M. Levine. An active foveated vision system: Attentional mechanisms and scan path convergence measures. *Comput. Vis. Image Underst.*, 63:50–65, 1996.
- [7] Simon Prince, James Elder, Yuqian Hou, Mikhail Sizintsev, and Yevgen Olevskiy. Statistical cue integration for foveated wide-field surveillance. volume 2, pages 603–610, 01 2005.
- [8] Ross Girshick, Jeff Donahue, Trevor Darrell, and Jitendra Malik. Rich feature hierarchies for accurate object detection and semantic segmentation. In *2014 IEEE Conference on Computer Vision and Pattern Recognition*, pages 580–587, 2014.
- [9] Shaoqing Ren, Kaiming He, Ross B. Girshick, and J. Sun. Faster r-cnn: Towards real-time object detection with region proposal networks. *IEEE Transactions on Pattern Analysis and Machine Intelligence*, 39:1137–1149, 2015.
- [10] Volodymyr Mnih, Nicolas Heess, Alex Graves, and Koray Kavukcuoglu. Recurrent models of visual attention. In *Proceedings of the 27th International Conference on Neural Information Processing Systems - Volume 2, NIPS’14*, page 2204–2212, Cambridge, MA, USA, 2014. MIT Press.
- [11] Christof Koch and Shimon Ullman. *Shifts in Selective Visual Attention: Towards the Underlying Neural Circuitry*, pages 115–141. Springer Netherlands, Dordrecht, 1987.
- [12] L. Itti, C. Koch, and E. Niebur. A model of saliency-based visual attention for rapid scene analysis. *IEEE Transactions on Pattern Analysis and Machine Intelligence*, 20(11):1254–1259, 1998.
- [13] Laurent Itti and Christof Koch. A saliency-based search mechanism for overt and covert shifts of visual attention. *Vision Research*, 40(10):1489–1506, 2000.
- [14] Hugo Touvron, Matthieu Cord, Matthijs Douze, Francisco Massa, Alexandre Sablayrolles, and Hervé Jégou. Training data-efficient image transformers & distillation through attention. *arXiv preprint arXiv:2012.12877*, 2020.
- [15] Alexey Dosovitskiy, Lucas Beyer, Alexander Kolesnikov, Dirk Weissenborn, Xiaohua Zhai, Thomas Unterthiner, Mostafa Dehghani, Matthias Minderer, Georg Heigold, Sylvain Gelly, Jakob Uszkoreit, and Neil Houlsby. An image is worth 16x16 words: Transformers for image recognition at scale. *arXiv preprint arXiv:2010.11929*, 2020.
- [16] Ashish Vaswani, Noam Shazeer, Niki Parmar, Jakob Uszkoreit, Llion Jones, Aidan N. Gomez, undefinedukasz Kaiser, and Illia Polosukhin. Attention is all you need. In *Proceedings of the 31st International Conference on Neural Information Processing Systems, NIPS’17*, page 6000–6010, Red Hook, NY, USA, 2017. Curran Associates Inc.
- [17] Jia Deng, Wei Dong, Richard Socher, Li-Jia Li, Kai Li, and Li Fei-Fei. Imagenet: A large-scale hierarchical image database. In *2009 IEEE Conference on Computer Vision and Pattern Recognition*, pages 248–255, 2009.
- [18] Chen Sun, Abhinav Shrivastava, Saurabh Singh, and Abhinav Gupta. Revisiting unreasonable effectiveness of data in deep learning era. In *2017 IEEE International Conference on Computer Vision (ICCV)*, pages 843–852, 2017.

- [19] Hugo Larochelle and Geoffrey E Hinton. Learning to combine foveal glimpses with a third-order boltzmann machine. In J. Lafferty, C. Williams, J. Shawe-Taylor, R. Zemel, and A. Culotta, editors, *Advances in Neural Information Processing Systems*, volume 23. Curran Associates, Inc., 2010.
- [20] Jimmy Ba, Volodymyr Mnih, and Koray Kavukcuoglu. Multiple object recognition with visual attention. In *ICLR (Poster)*, 2015.
- [21] Kelvin Xu, Jimmy Ba, Ryan Kiros, Kyunghyun Cho, Aaron Courville, Ruslan Salakhudinov, Rich Zemel, and Yoshua Bengio. Show, attend and tell: Neural image caption generation with visual attention. In Francis Bach and David Blei, editors, *Proceedings of the 32nd International Conference on Machine Learning*, volume 37 of *Proceedings of Machine Learning Research*, pages 2048–2057, Lille, France, 07–09 Jul 2015. PMLR.
- [22] Karol Gregor, Ivo Danihelka, Alex Graves, Danilo Rezende, and Daan Wierstra. Draw: A recurrent neural network for image generation. In Francis Bach and David Blei, editors, *Proceedings of the 32nd International Conference on Machine Learning*, volume 37 of *Proceedings of Machine Learning Research*, pages 1462–1471, Lille, France, 07–09 Jul 2015. PMLR.
- [23] Michal Gregor, Dušan Nemec, Aleš Janota, and Rastislav Pirník. A visual attention operator for playing pac-man. In *2018 ELEKTRO*, pages 1–6, 2018.
- [24] Aude Oliva and Antonio Torralba. Modeling the shape of the scene: A holistic representation of the spatial envelope. *International Journal of Computer Vision*, 42(3):145–175, May 2001.
- [25] Ruth Rosenholtz, Jie Huang, and Krista Ehinger. Rethinking the role of top-down attention in vision: Effects attributable to a lossy representation in peripheral vision. *Frontiers in Psychology*, 3:13, 2012.
- [26] Antonio Torralba, Aude Oliva, Monica Castelhana, and John Henderson. Contextual guidance of eye movements and attention in real-world scenes: The role of global features in object search. *Psychological review*, 113:766–86, 11 2006.
- [27] J. Freeman and E. Simoncelli. Metamers of the ventral stream. pages 1195–1201. *Nature Neuroscience*, 2011.
- [28] Emre Akbas and Miguel P. Eckstein. Object detection through search with a foveated visual system. *PLOS Computational Biology*, 13(10):1–28, 10 2017.
- [29] Kristie R. Dukewich and Raymond M. Klein. Inhibition of return: A phenomenon in search of a definition and a theoretical framework. *Attention, Perception, & Psychophysics*, 77(5):1647–1658, Jul 2015.
- [30] Diederik Kingma and Jimmy Ba. Adam: A method for stochastic optimization. *International Conference on Learning Representations*, 12 2014.
- [31] I. Loshchilov and F. Hutter. Decoupled weight decay regularization. In *ICLR*, 2019.
- [32] Yan Luo, Xavier Boix, Gemma Roig, Tomaso Poggio, and Qi Zhao. Foveation-based mechanisms alleviate adversarial examples. 11 2015.
- [33] Arturo Deza, Aditya Jonnalagadda, and Miguel Eckstein. Towards metamerism via foveated style transfer. 05 2017.
- [34] Arturo Deza and Talia Konkle. Emergent properties of foveated perceptual systems, 06 2020.
- [35] Taro Kiritani and Koji Ono. Recurrent attention model with log-polar mapping is robust against adversarial attacks, 02 2020.
- [36] Manish Reddy Vuyyuru, Andrzej Banburski, Nishka Pant, and Tomaso Poggio. Biologically inspired mechanisms for adversarial robustness. In H. Larochelle, M. Ranzato, R. Hadsell, M. F. Balcan, and H. Lin, editors, *Advances in Neural Information Processing Systems*, volume 33, pages 2135–2146. Curran Associates, Inc., 2020.
- [37] Ian Goodfellow, Jonathon Shlens, and Christian Szegedy. Explaining and harnessing adversarial examples. *arXiv 1412.6572*, 12 2014.
- [38] Alexey Kurakin, Ian Goodfellow, and Samy Bengio. Adversarial examples in the physical world. 07 2016.
- [39] Aleksander Madry, Aleksandar Makelov, Ludwig Schmidt, Dimitris Tsipras, and Adrian Vladu. Towards deep learning models resistant to adversarial attacks. 06 2017.

- [40] Nicolas Papernot, Fartash Faghri, Nicholas Carlini, Ian Goodfellow, Reuben Feinman, Alexey Kurakin, Cihang Xie, Yash Sharma, Tom Brown, Aurko Roy, Alexander Matyasko, Vahid Behzadan, Karen Hambardzumyan, Zhishuai Zhang, Yi-Lin Juang, Zhi Li, Ryan Sheatsley, Abhibhav Garg, Jonathan Uesato, Willi Gierke, Yinpeng Dong, David Berthelot, Paul Hendricks, Jonas Rauber, and Rujun Long. Technical report on the cleverhans v2.1.0 adversarial examples library. *arXiv preprint arXiv:1610.00768*, 2018.